On the phenomenology of a two-Higgs-doublet model with maximal CP symmetry at the LHC
II: radiative effects

M. Maniatis* and O. Nachtmann†
Institut für Theoretische Physik, Philosophenweg 16, 69120 Heidelberg, Germany

The processes $p\bar{p} \to \gamma +$heavy-flavour jet(s)$+X$ and $pp \to \gamma +$heavy-flavour jet(s)$+X$ are studied in the framework of a special two-Higgs-doublet model, the MCPM. As distinguishing feature of this model we find that radiative Higgs-boson production and decay lead to heavy flavour c jets but no b jets in the above processes. Thus, the prediction is that b jets should be given by the normal QCD processes whereas for c jets an excess over the QCD expectation should occur. We present results both for Tevatron and LHC energies.

1. INTRODUCTION

Two-Higgs-doublet models (THDMs) have been studied extensively since many years (see [1, 2, 3, 4, 5, 6, 7, 8, 9, 10, 11, 12, 13, 14, 15, 16, 17, 18, 19, 20] and references therein). These models provide a simple extension of the Standard Model of particle physics (SM) with a rich phenomenology due to the extended Higgs sector. In our group we have studied various aspects of the general multi-Higgs models and THDMs in particular [21, 22, 23, 24]. A special two-Higgs doublet model, the *maximally-CP-symmetric model* (MCPM), was introduced in [25, 26]. The phenomenology of the MCPM for high-energy proton–antiproton and proton–proton collisions was developed in detail in [27]. In the present article we continue the discussion of the MCPM phenomenology in view of processes involving real photons plus heavy flavour jets in the final state. That is, we consider the processes

$$p + \bar{p} \longrightarrow \gamma + \text{heavy-flavour jet(s)} + X\,, \tag{1}$$

relevant for the Tevatron physics, and

$$p + p \longrightarrow \gamma + \text{heavy-flavour jet(s)} + X \tag{2}$$

relevant for the LHC.

The general motivation for the MCPM is summarised in [27]. This will not be repeated her since the present paper is a direct continuation of this work. Let us recall from [27] that in the MCPM we have – as in every THDM – five physical Higgs bosons, three neutral ones and a charged pair:

$$\rho', \quad h', \quad h'', \quad H^\pm\,. \tag{3}$$

Distinguishing features of the MCPM as discussed in [27] are as follows.

- The Higgs bosons h', h'', and $H^\pm$ couple exclusively to the second fermion family (ν_μ, μ, c, s), but with coupling constants proportional to the masses of the third fermion family (ν_τ, τ, t, b).
- For Higgs-boson masses below about 300 GeV the ρ' behaves essentially as the Higgs boson $\rho'_{\rm SM}$ of the SM.
- The main decays of the other Higgs bosons are

$$h' \longrightarrow c\bar{c}\,, \qquad h'' \longrightarrow c\bar{c}\,, \qquad H^+ \longrightarrow c\bar{s}\,, \qquad H^- \longrightarrow s\bar{c}\,. \tag{4}$$

*E-mail: M.Maniatis@thphys.uni-heidelberg.de
†E-mail: O.Nachtmann@thphys.uni-heidelberg.de

- The main production modes of these Higgs bosons in high energy $p\bar{p}$ and pp collisions are Drell–Yan-type processes, that is, quark–antiquark fusion giving a Higgs boson.

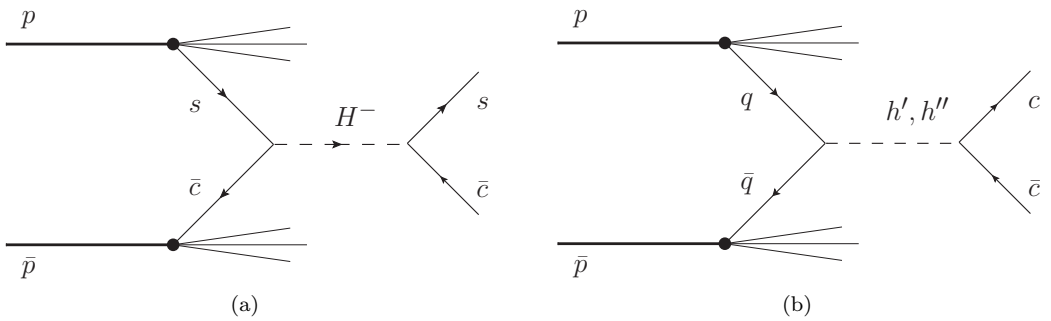

FIG. 1: (a): Drell–Yan process for production of a Higgs-boson H^- by $s\bar{c}$ fusion followed by the decay $H^- \longrightarrow s\bar{c}$. (b): Drell–Yan process for production of the Higgs-bosons h' and h'' with $q\bar{q}$ fusion where $q = s$ and c. This is followed by the decays $h' \longrightarrow c\bar{c}$ and $h'' \longrightarrow c\bar{c}$, respectively.

In Fig.1a we show the diagram for the Drell–Yan production of the H^- followed by its main decay for $p\bar{p}$ collisions. For pp collisions one just has to replace $\bar{p}$ by p. For the H^+ production and decay the replacements $s \to \bar{s}$ and $\bar{c} \to c$ have to be made. In Fig. 1b the Drell–Yan production processes of h' and h'' are shown followed by their main decays. The cross sections for these processes were calculated in [27]. For Higgs-boson masses of 100 to 300 GeV we find cross sections of order 300 to 1 pb for $p\bar{p}$ collisions at c.m energy 1.96 TeV. For pp collisions at c.m. energy 14 TeV these cross sections are of order 5000 to 500 pb. All these are relatively large cross sections.

The aim of the present article is to calculate the processes as shown in Figs. 1a and 1b but with the additional emission of a real photon. Clearly, this will lead to a photon plus one or two charm-quark jets in the final state. The distinguishing feature of the MCPM is that, as far as heavy quark flavours are concerned, only charm-quark jets are produced by this mechanism, no bottom-quark jets.

Our paper is organised as follows. In Sect. 2 we discuss the radiative production and the radiative decay of $H^\pm$. The analogous processes for the neutral Higgs bosons h' and h'' are studied in Sect. 3. In Sect. 4 we present numerical results. In Sect. 5 we discuss the possible relevance of our results in view of experimental results [28] from the Tevatron and we present our conclusions. The appendix contains details of our calculations. All our notations and kinematic conventions are the same as in [27] and follow [29].

2. RADIATIVE PRODUCTION OF $H^\pm$ AND $H^\pm$ RADIATIVE DECAY

In this section we discuss first the real photon emission in H^- production and decay as shown in Fig. 1a. Treating the s and $\bar{c}$ quarks as on-shell particles we have in lowest order of the electromagnetic coupling $e = \sqrt{4\pi\alpha_{\rm em}}$ five possibilities to attach a photon line to the basic diagram of Fig. 1a. This is shown in Fig. 2. In the following we shall always work in the narrow width approximation for the Higgs bosons. Then the diagrams of Fig. 2 can be considered as representing two distinct processes. We have firstly the radiative production of a *real* H^-

$$s(p_1') + \bar{c}(p_2') \longrightarrow H^-(k_1) + \gamma(k_2)\,. \tag{5}$$

The H^- decays then to a $s\bar{c}$ quark pair $H^- \longrightarrow s\bar{c}$. The diagrams (a), (b), and (c) of Fig. 2 contribute to (5).

Secondly, we have the Drell–Yan production of a *real* H^- which then decays to $s\bar{c}\gamma$:

$$H^-(k_1) \longrightarrow s(p_1') + \bar{c}(p_2') + \gamma(k_2)\,. \tag{6}$$

To (6) the diagrams (c), (d), and (e) of Fig. 2 contribute.

In this section we shall give the results for the processes (5) and (6). The details of the calculation are given in appendix A.

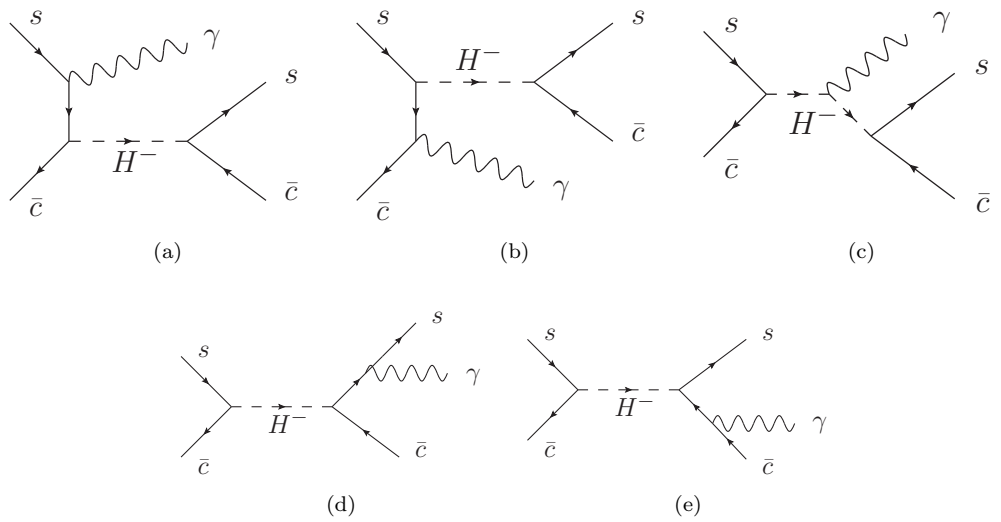

FIG. 2: The five diagrams for real photon emission in the basic Drell–Yan process of H^- production and decay of Fig. 1a.

2.1. Radiative $H^\pm$ production

The transition rate for radiative H^- production (5) is easily calculated. We get

$$d\Gamma\big(s(p_1')+\bar{c}(p_2')\to\ H^-(k_1)+\gamma(k_2)\big)=\frac{1}{V}\frac{1}{2p_1'^0 2p_2'^0}\frac{1}{(2\pi)^2}\frac{1}{4N_c^2}$$
$$\times\ I_{s\bar{c}}^{H^-}(p_1',p_2',k_1,k_2)\delta^{(4)}(p_1'+p_2'-k_1-k_2)\frac{d^3k_1}{2k_1^0}\frac{d^3k_2}{2k_2^0}\,, \quad (7)$$

where $N_c=3$ is the number of colours, V is the normalisation volume, and the function $I_{s\bar{c}}^{H^-}$ is given in appendix A. Using (7) we can, in the usual way, see for instance [29], calculate the Drell–Yan production of $H^-+\gamma$ in $p\bar{p}$ collisions

$$p(p_1)+\bar{p}(p_2)\longrightarrow\ H^-(k_1)+\gamma(k_2)+X\,. \quad (8)$$

We get for the cross section (for $p\bar{p}$ c.m. energy squared $s=(p_1+p_2)^2\gg m_p^2$) the following

$$d\sigma\big(p(p_1)+\bar{p}(p_2)\longrightarrow\ H^-(k_1)+\gamma(k_2)+X\big)=\frac{1}{2s}\frac{1}{4N_c^2}\frac{1}{(2\pi)^2}$$
$$\times\int_0^1 dx_1\int_0^1 dx_2\Big\{\frac{1}{x_1}N_s^p(x_1)\frac{1}{x_2}N_{\bar{c}}^{\bar{p}}(x_2)I_{s\bar{c}}^{H^-}(x_1p_1,x_2p_2,k_1,k_2)+\frac{1}{x_1}N_{\bar{c}}^p(x_1)\frac{1}{x_2}N_s^{\bar{p}}(x_2)I_{s\bar{c}}^{H^-}(x_2p_2,x_1p_1,k_1,k_2)\Big\}$$
$$\times\,\delta^{(4)}(x_1p_1+x_2p_2-k_1-k_2)\frac{d^3k_1}{2k_1^0}\frac{d^3k_2}{2k_2^0}\,. \quad (9)$$

Here $N_q^p(x)$ and $N_q^{\bar{p}}(x)$ are the usual parton distribution functions (pdf's) at the c.m. energy scale $\sqrt{s}$ considered.

In a similar way we can calculate the cross section for the H^+ production in $p\bar{p}$ collisions

$$p(p_1)+\bar{p}(p_2)\longrightarrow\ H^+(k_1)+\gamma(k_2)+X\,. \quad (10)$$

Here the basic process is

$$\bar{s}(p_1')+c(p_2')\longrightarrow\ H^+(k_1)+\gamma(k_2)\,. \quad (11)$$

The cross section for (10) is given by

$$d\sigma\big(p(p_1)+\bar{p}(p_2)\longrightarrow\ H^+(k_1)+\gamma(k_2)+X\big)=\frac{1}{2s}\frac{1}{4N_c^2}\frac{1}{(2\pi)^2}$$
$$\times\int\limits_0^1 dx_1\int\limits_0^1 dx_2\bigg\{\frac{1}{x_1}N_{\bar{s}}^p(x_1)\frac{1}{x_2}N_c^{\bar{p}}(x_2)I_{\bar{s}c}^{H^+}(x_1p_1,x_2p_2,k_1,k_2)+\frac{1}{x_1}N_c^p(x_1)\frac{1}{x_2}N_{\bar{s}}^{\bar{p}}(x_2)I_{\bar{s}c}^{H^+}(x_2p_2,x_1p_1,k_1,k_2)\bigg\}$$
$$\times\,\delta^{(4)}(x_1p_1+x_2p_2-k_1-k_2)\frac{d^3k_1}{2k_1^0}\frac{d^3k_2}{2k_2^0}\,, \quad (12)$$

where, as shown in appendix A,

$$I_{\bar{s}c}^{H^+}(p_1',p_2',k_1,k_2)=I_{s\bar{c}}^{H^-}(p_1',p_2',k_1,k_2)\,. \quad (13)$$

For the processes

$$p(p_1)+p(p_2)\longrightarrow\ H^\mp(k_1)+\gamma(k_2)+X \quad (14)$$

the cross sections read as in (9) and (12) with the replacements

$$N_{\bar{q}}^{\bar{p}}\longrightarrow N_{\bar{q}}^p,\qquad N_q^{\bar{p}}\longrightarrow N_q^p\,, \quad (15)$$

where $q=s,c$.

In Sect. 4 we shall give numerical results for the distributions in the transverse photon momentum $p_{\rm T}^\gamma=|\mathbf{k}_{2\rm T}|$ for the processes considered above.

2.2. Radiative decays of $H^\mp$

Here we study the decays

$$H^-(k_1)\longrightarrow\ s(p_1')+\bar{c}(p_2')+\gamma(k_2) \quad (16)$$

and

$$H^+(k_1)\longrightarrow\ \bar{s}(p_1')+c(p_2')+\gamma(k_2)\,. \quad (17)$$

The calculations presented in appendix A give for the differential decay rates

$$d\Gamma\big(H^-(k_1)\to\ s(p_1')+\bar{c}(p_2')+\gamma(k_2)\big)=\frac{1}{2m_{H^-}}\frac{1}{(2\pi)^5}\,\tilde{I}_{s\bar{c}}^{H^-}(p_1',p_2',k_1,k_2)$$
$$\times\,\delta^{(4)}(p_1'+p_2'+k_2-k_1)\frac{d^3p_1'}{2p_1'^0}\frac{d^3p_2'}{2p_2'^0}\frac{d^3k_2}{2k_2^0}\,, \quad (18)$$

$$d\Gamma\big(H^+(k_1)\to\ \bar{s}(p_1')+c(p_2')+\gamma(k_2)\big)=\frac{1}{2m_{H^+}}\frac{1}{(2\pi)^5}\,\tilde{I}_{\bar{s}c}^{H^+}(p_1',p_2',k_1,k_2)$$
$$\times\,\delta^{(4)}(p_1'+p_2'+k_2-k_1)\frac{d^3p_1'}{2p_1'^0}\frac{d^3p_2'}{2p_2'^0}\frac{d^3k_2}{2k_2^0}\,. \quad (19)$$

Here the CP and crossing symmetry relations give (see appendix A)

$$\tilde{I}_{s\bar{c}}^{H^-}(p_1',p_2',k_1,k_2)=\tilde{I}_{\bar{s}c}^{H^+}(p_1',p_2',k_1,k_2)=I_{s\bar{c}}^{H^-}(p_1',p_2',k_1,-k_2) \quad (20)$$

with $k_1=p_1'+p_2'+k_2$ due to energy-momentum conservation.

In Sect. 4 we shall use (18) and (19) to get the contribution to the γ flux from the ordinary Drell–Yan production of H^- and H^+ followed by the radiative decays (16) and (17), respectively.

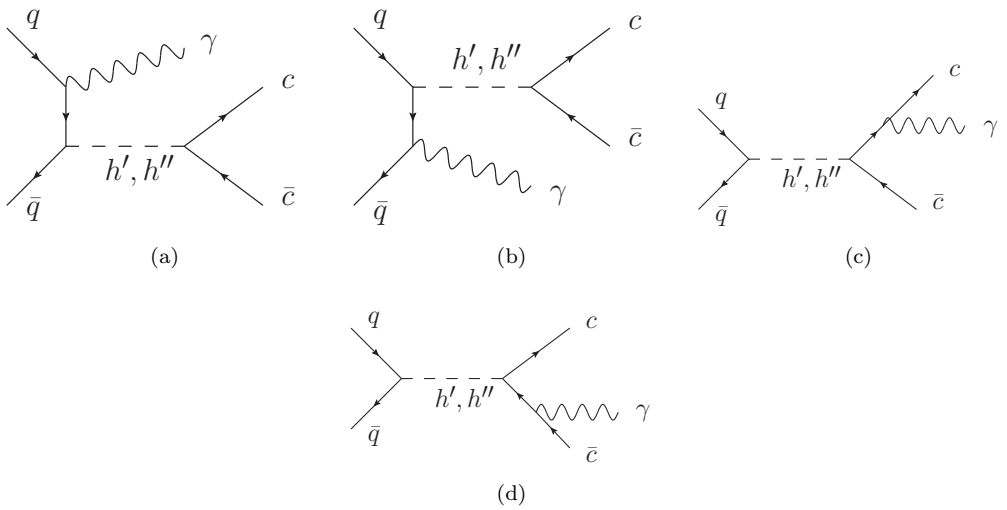

FIG. 3: The four diagrams for real photon emission in the basic Drell–Yan process for h' and h'' production and decay of Fig. 1b. Here $q = s, c$.

3. RADIATIVE PRODUCTION AND RADIATIVE DECAY OF h' AND h''

The Drell–Yan production of h' and h'' followed by the main decay of these bosons is shown in Fig. 1b. The corresponding diagrams for the process with emission of a real photon in addition are shown in Fig. 3.

We use the narrow width approximation for h' and h'' as for $H^{\pm}$. The diagrams (a) and (b) of Fig. 3 correspond then to the production of a *real* h' and h'' which subsequently decays to a $c\bar{c}$ pair

$$q(p_1') + \bar{q}(p_2') \longrightarrow h(k_1) + \gamma(k_2)\,. \tag{21}$$

Here and in the following we write generically h for h' and h''. The diagrams (c) and (d) of Fig. 3 correspond to the ordinary Drell–Yan production of h followed by the radiative decay

$$h(k_1) \longrightarrow c(p_1') + \bar{c}(p_2') + \gamma(k_2)\,. \tag{22}$$

The calculations for the process (21) are straightforward; see appendix A. The results for the process

$$p(p_1) + \bar{p}(p_2) \longrightarrow h(k_1) + \gamma(k_2) + X \tag{23}$$

are as follows:

$$\begin{aligned} d\sigma\big(p(p_1) + \bar{p}(p_2) \longrightarrow h(k_1) + \gamma(k_2) + X\big) &= \frac{1}{2s}\frac{1}{4N_c^2}\frac{1}{(2\pi)^2} \\ \times \int_0^1 dx_1 \int_0^1 dx_2 \Big\{ \sum_{q=s,c} \Big[\frac{1}{x_1} N_q^p(x_1) \frac{1}{x_2} N_{\bar{q}}^{\bar{p}}(x_2) I_{q\bar{q}}^h(x_1 p_1, x_2 p_2, k_1, k_2) + \frac{1}{x_1} N_{\bar{q}}^p(x_1) \frac{1}{x_2} N_q^{\bar{p}}(x_2) I_{q\bar{q}}^h(x_2 p_2, x_1 p_1, k_1, k_2) \Big] \Big\} \\ \times \delta^{(4)}(x_1 p_1 + x_2 p_2 - k_1 - k_2) \frac{d^3k_1}{2k_1^0} \frac{d^3k_2}{2k_2^0}\,. \end{aligned} \tag{24}$$

The functions $I_{q\bar{q}}^h$ are given in (A.12) and (A.13).

For the radiative decays

$$h(k_1) \longrightarrow q(p_1') + \bar{q}(p_2') + \gamma(k_2) \tag{25}$$

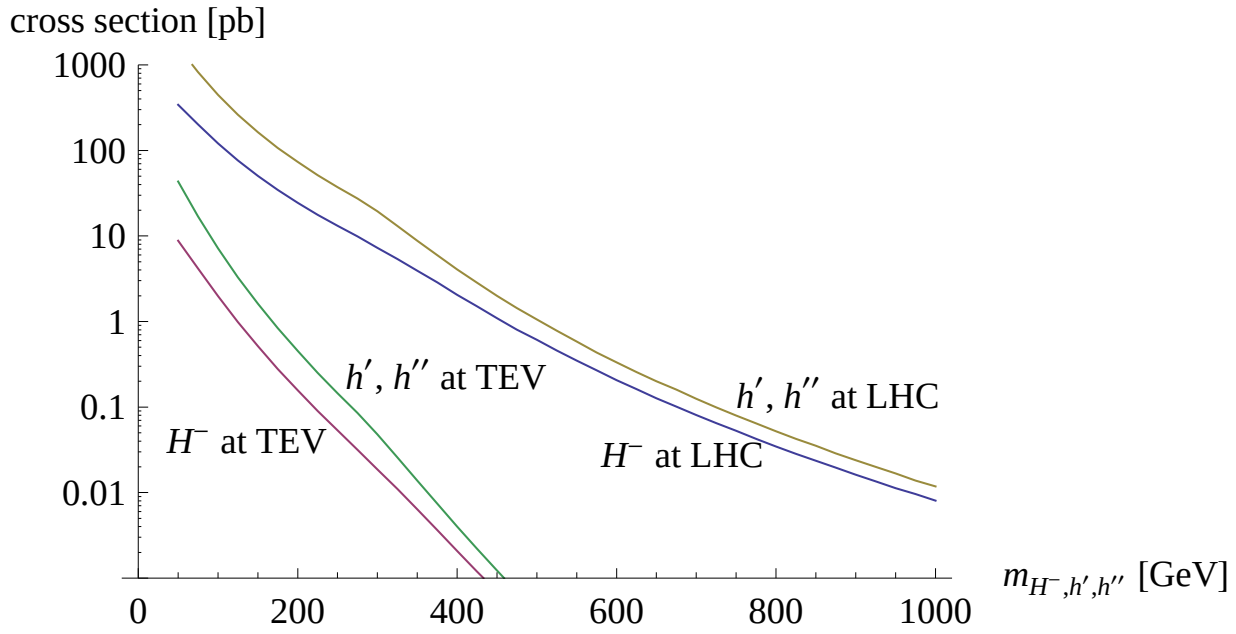

FIG. 4: Total cross sections for radiative Higgs-boson production and decay as functions of the Higgs-boson masses. The results are for Tevatron (lower curves) and LHC (upper curves) energies, 1.96 and 14 TeV, respectively.

with $q = s, c$ we get

$$d\Gamma\big(h(k_1) \to \ q(p_1') + \bar{q}(p_2') + \gamma(k_2)\big) = \frac{1}{2m_h}\frac{1}{(2\pi)^5}\ \tilde{I}^h_{q\bar{q}}(p_1', p_2', k_1, k_2)\delta^{(4)}(p_1' + p_2' + k_2 - k_1)\frac{d^3p_1'}{2p_1'^0}\frac{d^3p_2'}{2p_2'^0}\frac{d^3k_2}{2k_2^0}\ . \quad (26)$$

Here we have from appendix A

$$\tilde{I}^h_{q\bar{q}}(p_1', p_2', k_1, k_2) = I^h_{q\bar{q}}(p_1', p_2', k_1, -k_2)\,. \quad (27)$$

4. NUMERICAL RESULTS

In this section we present the numerical results for radiative Higgs-boson production and decay at Tevatron and LHC. As discussed in the introduction our calculation is performed in the narrow width approximation for the Higgs bosons. Then we always have two contributions which must be added incoherently: on the one hand we have Drell–Yan production of a single Higgs boson with its subsequent radiative decay into a quark pair and a photon. On the other hand we have radiative Higgs-boson production with subsequent decay of the Higgs boson into a quark pair.

In Fig. 4 we present the total cross sections calculated for the Tevatron ($\sqrt{s} = 1.96$ TeV) and the LHC ($\sqrt{s} = 14$ TeV) energies as functions of the Higgs-boson masses. For $p\bar{p}$ collisions the H^+ and H^- cross sections are equal; for pp collisions they are practically the same, since the s and $\bar{s}$ as well as the c and $\bar{c}$ pdf's are nearly equal. In order to avoid collinear and soft regions in phase space we apply a cut on the invariant scalar products of the relevant momenta p contracted with the photon momentum

$$(p\ k_2) \geq \mu\ , \quad (28)$$

where p stands for all initial and final state quark momenta as well as for the momentum of the Higgs-boson, $p = p_1', p_2', k_1$. We fix this minimal cut to $\mu = 100$ GeV^2. Note that in the limit of vanishing masses for the s- and c-quarks the cross sections for radiative h' and h'' production are equal; see appendix A. With increasing Higgs-boson masses we find a steep decrease of the total cross sections over several orders of magnitude. For the Tevatron we get,

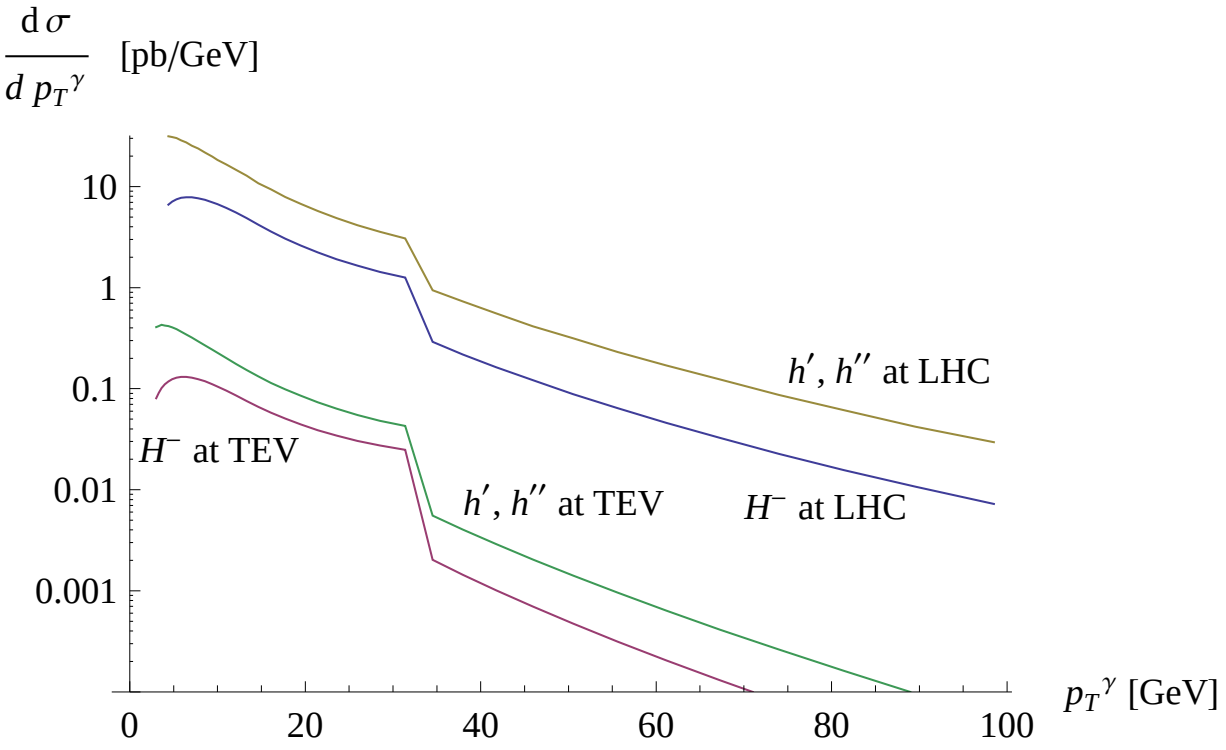

FIG. 5: Differential cross section $d\sigma/dp_{\rm T}^{\gamma}$ for radiative Higgs-boson production and decay at LHC (upper pair of curves) and Tevatron energies (lower pair of curves). The Higgs-boson mass is set to $m_{H^-/h'/h''} = 100$ GeV.

due to the much smaller available phase space, lower cross sections compared to those for the LHC. Nevertheless, even for the Tevatron energies the cross sections are not tiny, that is, above 0.1 pb for Higgs-boson masses below 200 GeV. At LHC energies the cross sections are larger than 0.1 pb for Higgs-boson masses up to about 600 GeV. Of course, the results depend strongly on the cut in the invariant scalar products, as discussed below. Note that the cross sections for the neutral Higgs bosons are larger than those for H^- by a factor of about two. This is due to the fact that for H^- production only $s\bar{c}$ annihilation but for h' and h'' both, $s\bar{s}$ and $c\bar{c}$ annihilation, contribute in proton–proton (LHC) respectively proton–antiproton (Tevatron) collisions; compare (9) with (24). But the cross sections for H^- and H^+ production taken together are similar to the individual cross sections for h' and h''. By a comparison of the radiative Higgs-boson cross sections to the Drell–Yan cross sections as discussed in [27] we find, as expected, the radiative cross sections suppressed by factors of order $\alpha_{\rm em}$.

In Figs. 5 and 6 we study the differential cross section $d\sigma/dp_{\rm T}^{\gamma}$ with respect to the transverse momentum of the photon. In Fig. 5 Higgs-boson masses of 100 GeV are assumed whereas in Fig. 6 we assume Higgs-boson masses of 200 GeV. Again a minimal invariant cut (28) with $\mu = 100$ GeV^2 is applied which leads to the suppression of the differential cross section for very low transverse momentum $p_{\rm T}^{\gamma}$, that is, below a few GeV. For increasing $p_{\rm T}^{\gamma}$ we find decreasing cross sections, as expected. An interesting feature of the $p_{\rm T}^{\gamma}$ distributions is the kink at large $p_{\rm T}^{\gamma}$ which is due to the fact that we have two contributions, the radiative Higgs-boson production and the Drell–Yan single Higgs-boson production with subsequent radiative decay. In our calculation we only consider the lowest order Drell–Yan single Higgs-boson production and neglect the transverse momenta of the quarks in the initial proton and antiproton. Then the transverse momentum of the singly produced Higgs boson is zero. It is clear that in the subsequent radiative decays of these Higgs bosons there is a maximal value for $p_{\rm T}^{\gamma}$, essentially half the Higgs-boson mass. Due to the cuts (28) this kinematic restriction is transformed into the kink at lower $p_{\rm T}^{\gamma}$ seen in Figs. 5 and 6. For values of $p_{\rm T}^{\gamma}$ above the kink in essence only radiative Higgs-boson production, that is, the processes (5), (11) and (21) contribute. In reality the kink will be washed out for several reasons: nonzero transverse momenta of the initial quarks; contributions to the Drell–Yan process at higher order in the strong coupling parameter α_s; finite width

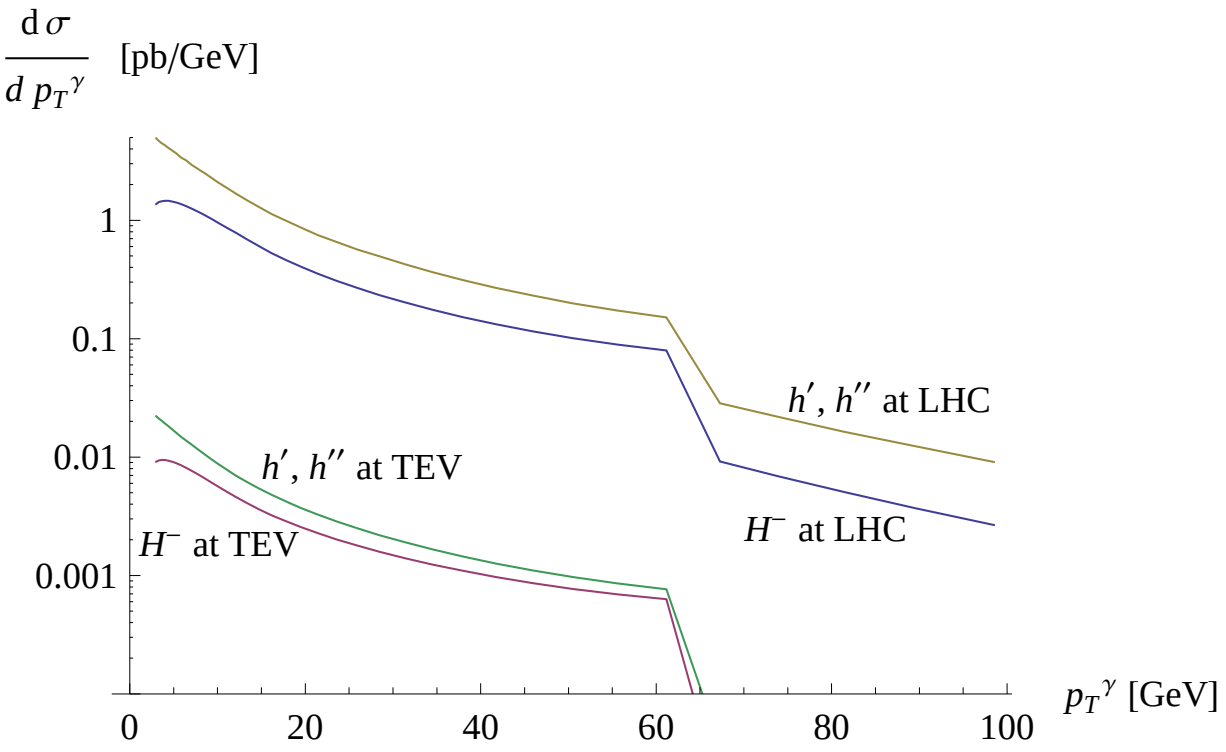

FIG. 6: Differential cross section $d\sigma/dp_{\mathrm{T}}^{\gamma}$ for radiative Higgs-boson production and decay at LHC (upper pair of curves) and Tevatron energies (lower pair of curves). The Higgs-boson mass is set to $m_{H^-/h'/h''} = 200$ GeV.

effects of the Higgs bosons.

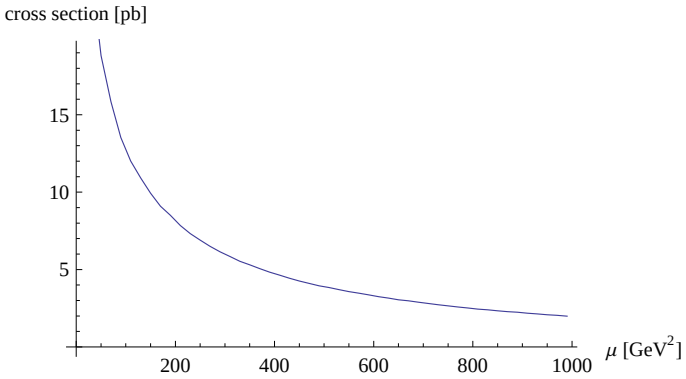

FIG. 7: Cross section for the charged Higgs-boson production $\sigma(p+p \to H^- + \gamma + X)$ at $\sqrt{s} = 14$ TeV as function of the the minimal invariant cut μ defined in (28). The charged Higgs-boson mass is set to $m_{H^-} = 200$ GeV.

Finally, we study in Fig. 7 the dependence of the cross sections on the invariant cut μ (28). As an example we show the radiative production cross section of a charged Higgs boson via the process $p+p \to H^- + \gamma + X$ at $\sqrt{s} = 14$ TeV as function of μ. As expected we get a steeply increasing cross section with decreasing cut parameter μ. Of course, the singularity in the limit of vanishing μ is not physical and would be absorbed by the corresponding virtual photon corrections to $p+p \to H^- + X$. In an experimental analysis of the processes (1) and (2) energy cuts and isolation cuts for the photon must reflect the real experimental conditions. Since such cuts are different for each experiment we have used here only the simple μ cut (28). But with the formulas given in the appendix any cuts can be implemented in a Monte Carlo program for experimental analysis.

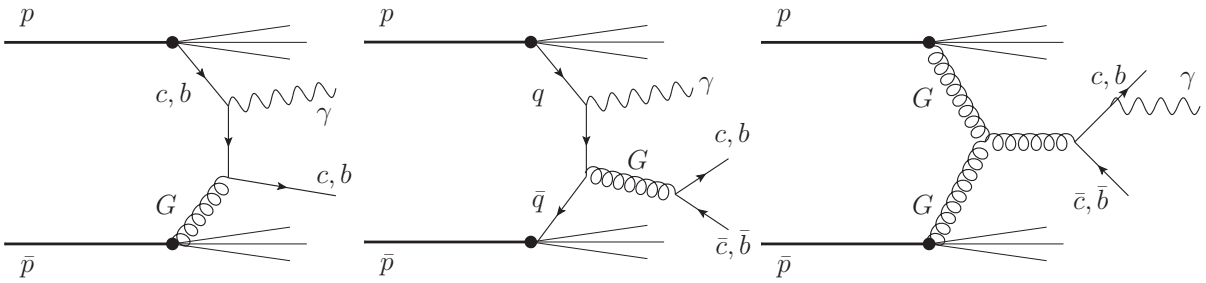

FIG. 8: Some typical QCD diagrams for processes contributing to $p + \bar{p} \to$ heavy flavour jet(s) $+ \gamma + X$.

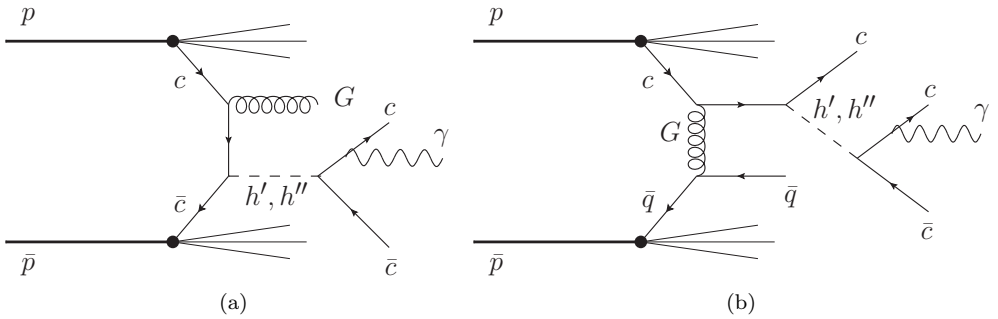

FIG. 9: (a): Example of a diagram giving a higher order QCD correction to the Drell–Yan production of h' and h''. (b): Example of a diagram where a Higgs boson h' or h'' is produced in a $c\bar{q}$ collision where q can be any quark flavour. These Higgs bosons may then decay radiatively.

5. CONCLUSIONS

In this article we have calculated the simplest processes contributing to radiative Higgs-boson production and decay in the MCPM for pp and $p\bar{p}$ collisions at high energies. As an interesting signal obtainable form these processes for experiments we discussed the inclusive production of heavy flavour jet(s) plus a real photon, see (1) and (2). In the MCPM only c-quark, no b-quark jets are produced from the Higgs channels. Of course, processes (1) and (2) also occur due to Standard Model QCD effects. Some diagrams for processes contributing in $p\bar{p}$ collisions are shown in Fig. 8. For pp collisions one just has to replace $\bar{p}$ by p. These QCD processes are a background to the Higgs-boson processes (see Figs. 2 and 3) studied in the present paper.

Let us emphasise as distinguishing feature of the MCPM that we predict only c and $\bar{c}$ quark jets from the Higgs-boson channels. Thus, the b and $\bar{b}$ jets in the processes (1) and (2) should show Standard Model QCD behaviour. In contrast, there should be a surplus of c and $\bar{c}$ jets over the QCD expectation. We note that due to different final states there is no interference of the diagrams of Figs. 2 and 3 with the dominant QCD diagrams, examples of which are given in Fig. 8. Thus, the QCD and Higgs-boson mediated contributions of the processes (1) and (2) must be added incoherently.

We found cross sections of order 0.1 to 50 pb for the radiative Higgs-boson production at the Tevatron energy $\sqrt{s} = 1.96$ TeV. But only for rather light Higgs bosons the cross section exceeds 1 pb; see Fig. 4. In contrast, at $\sqrt{s} = 14$ TeV to be reached at the LHC we predict large cross sections even for rather heavy Higgs bosons. For instance for Higgs-boson masses $h', h'', H^{\pm}$ of about 400 GeV we get cross sections exceeding 1 pb. For an integrated luminosity of 100 fb^{-1} at LHC this corresponds to at least 100,000 Higgs bosons being either produced radiatively or being produced and then decaying radiatively. Even if one order of magnitude of this number of Higgs bosons is lost due to the separation of the signal from the background this is still a sizable number which should be detectable at the LHC.

Let us note that recently experimental results for process (1) were published by the D0 collaboration at Fermilab [28]. This collaboration observes an excess over the QCD expectation for the cross section $\sigma(p\bar{p} \to \gamma + c + X)$ for photons with a transverse momentum exceeding 70 GeV. In contrast, no such excess is observed for the analogous process $\sigma(p\bar{p} \to \gamma + b + X)$. Qualitatively this finding is as expected in the MCPM. But what about the quantitative aspects? First of all we must mention that the statistical significance of the excess in the charm channel is only about 1.6 to 2.2σ. Thus, the effect may well go away with further measurements. But, for the sake of argument, let us take the observed charm jet excess seriously and try to see if it could have anything to to with the MCPM. The excess cross section $d\sigma/dp_{\rm T}^{\gamma}$ which one can deduce from Table I of [28] is of the order of 0.02 pb/GeV for $p_{\rm T}^{\gamma} = 70$ to 90 GeV. Comparing with our Figs. 5 and 6 we see that we find cross sections of this level only for $p_{\rm T}^{\gamma} < 20$ (10) GeV for a Higgs-boson mass of 100 (200) GeV. Thus, our calculated cross sections seems too low compared to the findings of [28]. But we have to keep in mind several points before we can draw definite conclusions.

We used different cuts in our calculations compared to the experiments. We would invite the experimentalists to use our formulas as given in the appendix and to include the processes studied in this paper into their Monte Carlo programs. Then all their experimental cuts can be implemented appropriately.

In the MCPM there are also further mechanisms which will contribute to the process (1). We have higher order QCD corrections to the Drell–Yan production of the Higgs bosons, see Fig. 9a. These processes are suppressed by a factor α_s relative to the leading order Drell–Yan process. But, clearly, diagrams as shown in Fig. 9a will lead to Higgs bosons produced at substantial values of $p_{\rm T}$. Then, the radiative decay of these Higgs bosons will lead to photons of much higher $p_{\rm T}^{\gamma}$ than from the leading order process. Furthermore there is the possibility of a sort of Higgs-strahlung process in $p\bar{p}$ collisions. An example in shown in Fig. 9b. Since the coupling of the c quark to h' and h'' is of order 1 the rates for such processes could be quite large. Clearly, for such processes there are the analogous radiative production ones which will also contribute to (1).

In summary we can say the following concerning the findings of [28]. If the charm excess seen is real and confirmed by further experiments it is not excluded that it may have something to do with Higgs-boson production in the MCPM. Our calculations of the cross sections and the $p_{\rm T}^{\gamma}$ distributions for the processes (1) and (2) must be considered as giving only lower limits for these quantities in the MCPM. We have identified above various channels which will also contribute but still have to be calculated theoretically. Nonetheless we can say that - at least to us - the magnitude of the effects calculated so far looks interesting for the Tevatron experiments. Thus, a study of the invariant mass distributions of the channels $c\bar{c}$, $c\bar{s}$, $s\bar{c}$, $c\bar{c}\gamma$, $c\bar{s}\gamma$, and $s\bar{c}\gamma$ could be interesting.

We hope that our remarks will be useful to experimentalists and will induce them to study further heavy flavour jet(s) plus photon inclusive production in $p\bar{p}$ and pp collisions at the Tevatron and the LHC, respectively.

Acknowledgments

We thank H. C. Schultz-Coulon for useful discussions. This work was supported by Deutsche Forschungsgemeinschaft, project number NA 296/5-1.

APPENDIX A

Here we give some details of the calculation for the radiative production and radiative decays of h', h'' and $H^{\pm}$.

Let us first consider the reaction (5) and the corresponding T-matrix element for production of a photon with polarisation vector ϵ

$$\epsilon^{*\mu} \mathcal{T}_{\mu}^{H^-} = \langle H^-(k_1), \gamma(k_2, \epsilon) \mid T \mid s(p_1'), \bar{c}(p_2') \rangle \ . \tag{A.1}$$

Here and in the following the colour and spin indices of the quarks are not written out explicitly. The function $I^{H^-}_{s\bar{c}}$ is defined as

$$I^{H^-}_{s\bar{c}}(p_1', p_2', k_1, k_2) = \sum_{\text{spins, colours}} (-1)\, \mathcal{T}^{H^-}_{\mu} (\mathcal{T}^{H^-\mu})^* \,. \tag{A.2}$$

The calculation of this squared amplitude for the process (5) is straightforward and yields

$$\begin{aligned}
I^{H^-}_{s\bar{c}}(p_1', p_2', k_1, k_2) = \frac{4e^2}{v_0^2} N_c \Bigg\{ & \\
& \frac{Q_s^2}{(p_1'k_2)^2}\Big[(m_t^2+m_b^2)((p_1'k_2)(p_2'k_2) - (p_1'p_2')m_s^2 + (p_2'k_2)m_s^2) + 2m_t m_b m_c m_s((p_1'k_2) - m_s^2)\Big] + \\
& \frac{Q_c^2}{(p_2'k_2)^2}\Big[(m_t^2+m_b^2)((p_1'k_2)(p_2'k_2) - (p_1'p_2')m_c^2 + (p_1'k_2)m_c^2) + 2m_t m_b m_c m_s((p_2'k_2) - m_c^2)\Big] + \\
& \frac{1}{(k_1k_2)^2}\Big[-(m_t^2+m_b^2)(p_1'p_2')(m_{H^-}^2 + (p_1'k_2) + (p_2'k_2)) - 2m_t m_b m_c m_s(m_{H^-}^2 + (p_1'k_2) + (p_2'k_2))\Big] + \\
& \frac{Q_sQ_c}{(p_1'k_2)(p_2'k_2)}\Big[(m_t^2+m_b^2)(2(p_1'p_2')^2 - 2(p_1'p_2')(p_1'k_2) - 2(p_1'p_2')(p_2'k_2) + 2(p_1'k_2)(p_2'k_2) + \\
& \qquad m_c^2(p_1'k_2) + m_s^2(p_2'k_2)) + 2m_t m_b m_c m_s(2(p_1'p_2') - (p_1'k_2) - (p_2'k_2))\Big] + \\
& \frac{Q_c}{(p_2'k_2)(k_1k_2)}\Big[(m_t^2+m_b^2)(2(p_1'p_2')^2 - 2(p_1'p_2')(p_1'k_2) - (p_1'p_2')(p_2'k_2) \\
& + 2m_c^2(p_1'p_2') - m_c^2(p_1'k_2) + m_s^2(p_2'k_2)) + 2m_t m_b m_c m_s(2(p_1'p_2') - (p_1'k_2) - 2(p_2'k_2) + 2m_c^2)\Big] + \\
& \frac{Q_s}{(p_1'k_2)(k_1k_2)}\Big[-(m_t^2+m_b^2)(2(p_1'p_2')^2 - 2(p_1'p_2')(p_2'k_2) - (p_1'p_2')(p_1'k_2) \\
& + 2m_s^2(p_1'p_2') + m_c^2(p_1'k_2) - m_s^2(p_2'k_2)) + 2m_t m_b m_c m_s(-2(p_1'p_2') + 2(p_1'k_2) + (p_2'k_2) - 2m_s^2)\Big]\Bigg\} \,.
\end{aligned} \tag{A.3}$$

Here $Q_s = -1/3$ and $Q_c = 2/3$ are the charges of the s and c quark in units of the positron charge, respectively. The standard Higgs-boson vacuum expectation value is $v_0 \approx 246$ GeV. The function $I^{H^-}_{s\bar{c}}$ is defined only for momenta satisfying energy-momentum conservation, $p_1' + p_2' = k_1 + k_2$.

We can always use energy-momentum conservation to eliminate one of the momenta in (A.3). Since the momentum one may want to eliminate differs from case to case we keep the more symmetric but redundant notation of (A.3). We have kept the masses of all quarks non-vanishing. Of course the expression (A.3) simplifies considerably if we neglect the s- and c-quark masses.

Next we consider the reaction (11). We can use the standard CP transformation to relate the amplitudes for the reactions (5) and (11). This transformation, denoted by $\mathrm{CP}_s \equiv \mathrm{CP}^{(ii)}_{g,2}$ in [26, 27], is conserved in the MCPM (see sect. 3 of [26]) and therefore we find

$$\epsilon^{*\mu}\mathcal{T}^{H^+}_{\mu} = \langle H^+(k_1), \gamma(k_2,\epsilon) \mid T \mid \bar{s}(p_1'), c(p_2')\rangle = \langle H^-(\tilde{k}_1), \gamma(\tilde{k}_2,\tilde{\epsilon}) \mid T \mid s(\tilde{p}_1'), \bar{c}(\tilde{p}_2')\rangle \tag{A.4}$$

where

$$\tilde{k}^{\lambda}_{1,2} = k_{1,2\,\lambda} \,, \qquad \tilde{p}^{'\lambda}_{1,2} = p'_{1,2\,\lambda} \,, \qquad \tilde{\epsilon}^{\lambda} = \epsilon_{\lambda} \,. \tag{A.5}$$

Analogously to (A.2) we define

$$I^{H^+}_{\bar{s}c}(p_1', p_2', k_1, k_2) = \sum_{\text{spins, colours}} (-1)\, \mathcal{T}^{H^+}_{\mu} (\mathcal{T}^{H^+\mu})^* \,. \tag{A.6}$$

and find from (A.2) and (A.4)

$$I^{H^+}_{\bar{s}c}(p_1', p_2', k_1, k_2) = I^{H^-}_{s\bar{c}}(\tilde{p}_1', \tilde{p}_2', \tilde{k}_1, \tilde{k}_2) \; . \tag{A.7}$$

Since $I^{H^-}_{s\bar{c}}$ depends only on three linearly independent four momenta there is no parity odd scalar which can be formed. Thus, we get

$$I^{H^-}_{s\bar{c}}(\tilde{p}_1', \tilde{p}_2', \tilde{k}_1, \tilde{k}_2) = I^{H^-}_{s\bar{c}}(p_1', p_2', k_1, k_2) \; , \tag{A.8}$$

as can also be verified directly form (A.3). Combining (A.7) and (A.8) we obtain

$$I^{H^+}_{\bar{s}c}(p_1', p_2', k_1, k_2) = I^{H^-}_{s\bar{c}}(p_1', p_2', k_1, k_2) \; . \tag{A.9}$$

For the reaction (21) we write the T-matrix element similarly to (A.1)

$$\epsilon^{*\mu}\mathcal{T}^h_{q\bar{q},\,\mu} = \langle h(k_1), \gamma(k_2, \epsilon) \mid T \mid q(p_1'), \bar{q}(p_2')\rangle \tag{A.10}$$

with $q = s, c$. The corresponding function $I^h_{q\bar{q}}$ is defined as

$$I^h_{q\bar{q}}(p_1', p_2', k_1, k_2) = \sum_{\text{spins, colours}} (-1)\; \mathcal{T}^h_{q\bar{q},\,\mu}(\mathcal{T}^{h\,\mu}_{q\bar{q}})^* \; . \tag{A.11}$$

This squared amplitude reads for $h = h'$

$$\begin{aligned} I^{h'}_{s\bar{s}/c\bar{c}}(p_1', p_2', k_1, k_2) = \left(\frac{Q_{s/c}\, e}{v_0}\right)^2 4N_c m^2_{b/t}\Bigg\{ \\ \frac{2}{(p_1'k_2)(p_2'k_2)}\left[(p_1'p_2')^2 - (p_1'p_2')(p_1'k_2) - (p_1'p_2')(p_2'k_2) + m^2_{s/c}(p_1'k_2) + m^2_{s/c}(p_2'k_2) - m^2_{s/c}(p_1'p_2')\right] \\ -\frac{m^2_{s/c}}{(p_1'k_2)^2}\left[(p_1'p_2')+(p_1'k_2)-(p_2'k_2)-m^2_{s/c}\right] - \frac{m^2_{s/c}}{(p_2'k_2)^2}\left[(p_1'p_2')-(p_1'k_2)+(p_2'k_2)-m^2_{s/c}\right] + \frac{1}{(p_1'k_2)(p_2'k_2)}\left[(p_1'k_2)+(p_2'k_2)\right]^2\Bigg\} . \end{aligned} \tag{A.12}$$

For $h = h''$ we find

$$\begin{aligned} I^{h''}_{s\bar{s}/c\bar{c}}(p_1', p_2', k_1, k_2) = \left(\frac{Q_{s/c}e}{v_0}\right)^2 4N_c m^2_{b/t}\Bigg\{ \\ \left[\frac{2(p_1'p_2')}{(p_1'k_2)(p_2'k_2)} - \frac{m^2_{s/c}}{(p_1'k_2)^2} - \frac{m^2_{s/c}}{(p_2'k_2)^2}\right]\left[(p_1'p_2') - (p_1'k_2) - (p_2'k_2) + m^2_{s/c}\right] + \frac{1}{(p_1'k_2)(p_2'k_2)}\left[(p_1'k_2) + (p_2'k_2)\right]^2\Bigg\}. \end{aligned} \tag{A.13}$$

We see that for vanishing masses $m_s = m_c = 0$ we have $I^{h''}_{s\bar{s}/c\bar{c}} = I^{h'}_{s\bar{s}/c\bar{c}}$.

Let us now discuss the radiative decays of H^- (16) and H^+ (17). We define the corresponding amplitudes as

$$\epsilon^{*\mu}\tilde{\mathcal{T}}^{H^-}_{\mu} = \langle s(p_1'), \bar{c}(p_2'), \gamma(k_2, \epsilon) \mid T \mid H^-(k_1)\rangle, \qquad \epsilon^{*\mu}\tilde{\mathcal{T}}^{H^+}_{\mu} = \langle \bar{s}(p_1'), c(p_2'), \gamma(k_2, \epsilon) \mid T \mid H^+(k_1)\rangle \; . \tag{A.14}$$

Next we define

$$\tilde{I}^{H^-}_{s\bar{c}}(p_1', p_2', k_1, k_2) = \sum_{\text{spins, colours}} (-1)\; \tilde{\mathcal{T}}^{H^-}_{\mu}(\tilde{\mathcal{T}}^{H^-\mu})^* \; , \quad \tilde{I}^{H^+}_{\bar{s}c}(p_1', p_2', k_1, k_2) = \sum_{\text{spins, colours}} (-1)\; \tilde{\mathcal{T}}^{H^+}_{\mu}(\tilde{\mathcal{T}}^{H^+\mu})^* \; . \tag{A.15}$$

It is easy to see that the following crossing relation holds

$$\tilde{\mathcal{T}}^{H^-}_{\mu} = (\mathcal{T}^{H^-}_{\mu})^*\big|_{k_2 \to -k_2} \; , \tag{A.16}$$

where $\mathcal{T}^{H^-}_{\mu}$ is defined in (A.1). From (A.16) and (A.2) we get immediately

$$\tilde{I}^{H^-}_{s\bar{c}}(p_1', p_2', k_1, k_2) = I^{H^-}_{s\bar{c}}(p_1', p_2', k_1, -k_2) \; , \tag{A.17}$$

where $k_1 = p_1' + p_2' + k_2$. The same CP arguments as used in (A.4) to (A.9) give also

$$\tilde{I}^{H^+}_{\bar{s}c}(p_1', p_2', k_1, k_2) = I^{H^-}_{s\bar{c}}(p_1', p_2', k_1, -k_2) \; . \tag{A.18}$$

Finally we discuss the decay

$$h(k_1) \to q(p_1') + \bar{q}(p_2') + \gamma(k_2, \epsilon) \; , \tag{A.19}$$

with $q = s,\ c$ and $h = h',\ h''$. The corresponding amplitude and the squared amplitude are defined as follows

$$\epsilon^{*\mu} \tilde{\mathcal{T}}^h_{q\bar{q},\,\mu} = \langle q(p_1'), \bar{q}(p_2'), \gamma(k_2, \epsilon) \mid T \mid h(k_1) \rangle \; , \tag{A.20}$$

$$\tilde{I}^h_{q\bar{q}}(p_1', p_2', k_1, k_2) = \sum_{\text{spins, colours}} (-1)\, \tilde{\mathcal{T}}^h_{q\bar{q},\,\mu} (\tilde{\mathcal{T}}^{h\,\mu}_{q\bar{q}})^* \; , \tag{A.21}$$

With the same crossing arguments as used to derive (A.16) and (A.17) we find

$$\tilde{I}^h_{q\bar{q}}(p_1', p_2', k_1, k_2) = I^h_{q\bar{q}}(p_1', p_2', k_1, -k_2) \; , \tag{A.22}$$

where $k_1 = p_1' + p_2' + k_2$.

---

[1] M. Kobayashi and T. Maskawa, Prog. Theor. Phys. **49** 652 (1973)
[2] T. D. Lee, Phys. Rev. D **8** 1226 (1973).
[3] T. D. Lee, Phys. Rept. **9** 143 (1974) .
[4] S. L. Glashow and S. Weinberg, Phys. Rev. D **15** 1958 (1977).
[5] E. A. Paschos, Phys. Rev. D **15** 1966 (1977).
[6] J. F. Gunion, H. E. Haber, G. L. Kane and S. Dawson, "The Higgs Hunter's Guide", Addison–Wesley publishing company (1990).
[7] G. Cvetic, Phys. Rev. D **48** 5280 (1993) [hep-ph/9309202].
[8] I. F. Ginzburg and M. Krawczyk, Phys. Rev. D **72** 115013 (2005) [hep-ph/0408011].
[9] J. F. Gunion and H. E. Haber, Phys. Rev. D **72** 095002 (2005) [hep-ph/0506227v2].
[10] R. Barbieri and L. J. Hall, "Improved naturalness and the two Higgs doublet model", [hep-ph/0510243].
[11] G. C. Branco, M. N. Rebelo and J. I. Silva-Marcos, Phys. Lett. B **614** 187 (2005) [hep-ph/0502118].
[12] R. Barbieri, L. J. Hall and V. S. Rychkov, Phys. Rev. D **74** 015007 (2006) [hep-ph/0603188].
[13] C. C. Nishi, Phys. Rev. D **74**, 036003 (2006) [Erratum-ibid. D **76** 119901 (2007)] [arXiv:hep-ph/0605153].
[14] I. P. Ivanov, Phys. Rev. D **75**, 035001 (2007) [Erratum-ibid. D **76** 039902 (2007)] [arXiv:hep-ph/0609018].
[15] L. Fromme, S. J. Huber and M. Seniuch, JHEP **0611** 038 (2006) [hep-ph/0605242].
[16] A. Barroso, P. M. Ferreira and R. Santos, Phys. Lett. B **652** 181 (2007) [arXiv:hep-ph/0702098].
[17] J. M. Gerard and M. Herquet, Phys. Rev. Lett. **98** 251802 (2007) [hep-ph/0703051].
[18] E. Ma and M. Maniatis, arXiv:0909.2855 [hep-ph].
[19] P. M. Ferreira, H. E. Haber and J. P. Silva, Phys. Rev. D **79** 116004 (2009) [arXiv:0902.1537 [hep-ph]].
[20] F. Mahmoudi and O. Stal, arXiv:0907.1791 [hep-ph].
[21] W. Bernreuther and O. Nachtmann, Eur. Phys. J. C **9** 319 (1999) [arXiv:hep-ph/9812259].
[22] F. Nagel, "New aspects of gauge-boson couplings and the Higgs sector," (2004) SPIRES entry
[23] M. Maniatis, A. von Manteuffel, O. Nachtmann and F. Nagel, Eur. Phys. J. C **48** 805 (2006) [hep-ph/0605184].
[24] M. Maniatis, A. von Manteuffel and O. Nachtmann, Eur. Phys. J. C **49** 1067 (2007) [arXiv:hep-ph/0608314].
[25] M. Maniatis, A. von Manteuffel and O. Nachtmann, Eur. Phys. J. C **57** 719 (2008) [arXiv:0707.3344 [hep-ph]].
[26] M. Maniatis, A. von Manteuffel and O. Nachtmann, Eur. Phys. J. C **57** 739 (2008) [arXiv:0711.3760 [hep-ph]].
[27] M. Maniatis and O. Nachtmann, JHEP **0905** 028 (2009) [arXiv:0901.4341 [hep-ph]].
[28] V. M. Abazov *et al.* [D0 Collaboration], Phys. Rev. Lett. **102** 192002 (2009) [arXiv:0901.0739 [hep-ex]].
[29] O. Nachtmann, "Elementary Particle Physics: Concepts And Phenomena", Springer, Berlin (1990).